Rare variant effect estimation and polygenic risk prediction

Kisung Nam[1], Minjung Kho[1], Wei Zhou[2,3,4], Bhramar Mukherjee[5], Seunggeun Lee[1]

Abstract

Due to their low frequency, estimating the effect of rare variants is challenging. Here, we propose RareEffect, a method that first estimates gene- or region-based heritability and then each variant effect size using an empirical Bayes approach. Our method uses a variance component model, popular in rare variant tests, and is designed to provide two levels of effect sizes, gene/region-level and variant-level, which can provide better interpretation. To adjust for the case-control imbalance in phenotypes, our approach uses a fast implementation of the Firth bias correction. We demonstrate the accuracy and computational efficiency of our method through extensive simulations and the analysis of UK Biobank whole exome sequencing data for 100 traits. Additionally, we show that the effect sizes obtained from our model can be leveraged to improve the performance of polygenic scores, outperforming recently developed methods for rare variant polygenic scoring.

[1] Graduate School of Data Science, Seoul National University, Seoul, South Korea
[2] Psychiatric and Neurodevelopmental Genetics Unit, Center for Genomic Medicine, Massachusetts General Hospital, Boston, MA, USA
[3] Stanley Center for Psychiatric Research, Broad Institute of MIT and Harvard, Cambridge, MA, USA
[4] Program in Medical and Population Genetics, Broad Institute of MIT and Harvard, Cambridge, MA, USA
[5] Department of Biostatistics, Yale School of Public Health, Yale University, New Haven, CT, USA

Introduction

With the availability of extensive sequencing data in biobanks[1], the study of rare variants has become more feasible than ever before. Rare variants have been identified as potential causative factors for numerous complex diseases[2-8], and their exploration is crucial in unraveling the genetic risk factors of complex traits[9]. To identify the association between rare variants and complex traits, gene or region-based tests[10,11], including the Burden test, the sequence kernel association test (SKAT)[12] and its adaptive optimized version (SKAT-O)[13], have been commonly used. Recently, several methods, including STAAR[14], SAIGE-GENE[15], SAIGE-GENE+[16], and DeepRVAT[17] are developed to run region-based tests in biobank scale data.

To elucidate the effect of rare variants on complex diseases and traits and utilize them for risk prediction, in addition to calculating p-values for association tests, effect size estimation is required. However, estimating the effect size of rare variants remains a challenge. The low minor allele frequencies make single variant-based estimations unstable. Popular association tests like SKAT and SKAT-O are score tests, so only provide p-values. Although the Burden test provides a gene-burden effect size, this may not accurately reflect the true effect of rare variants in the presence of null variants and variants with opposing association directions. Recently, several methods have been developed to estimate the effect sizes of rare variants, aiming to overcome the limitations of burden test approaches[18-20]. However, these methods often require excessive computational resources, making their application to large-scale datasets impractical. Alternative approaches estimate burden effect sizes by weighting variants according to their predicted functional impact or by directly computing gene impairment scores from predicted variant functionality[17,21,22]. However, as variant function prediction remains an evolving field, such direct weighting strategies may be prone to reduced accuracy.

To address the challenges, we introduce RareEffect, a novel method that estimates gene or region-based heritability and subsequently calculates each variant's effect size using an empirical Bayes approach. Utilizing a variance component model, similar to that in the SKAT test, our method offers dual-level effect size estimation, region-level and variant-level, for enhanced interpretability. Unlike the Burden approach, our model flexibly estimates effect sizes in a data-driven manner. To reduce the computational burden for estimating variance

components, we implemented the Factored Spectrally Transformed Linear Mixed Models (FaST-LMM)[23], which leverages the low rank of the genetic relatedness matrix. We also utilize the strategy to collapse ultra-rare variants, as used in SAIGE-GENE+, to reduce the sparsity of the genotype matrix and improve power of estimating the effect of ultra-rare variants[16]. For binary traits, we additionally apply a fast implementation of the Firth bias reduction method to stably estimate the effect sizes.

From simulation studies, we showed that the proposed method is computationally fast and reliably estimates each gene heritability. We also showed that the proposed approach outperformed linear regression or ridge regression in terms of root mean squared error (RMSE) for estimating the individual-variant level effect sizes. From the UK Biobank (UKB) Whole Exome Sequencing (WES) data analysis of 100 traits, we demonstrate that exonic rare variants can explain additional phenotypic variabilities, but the degree differs by phenotypes. We also demonstrated that our approach explains phenotypic variability more effectively than recently developed methods based on predicted variant functional impact or gene-impairment scores, such as AlphaMissense[21], PrimateAI-3D[22] and DeepRVAT[17]. These findings provide strong evidence for the practical utility of our method in leveraging rare variant data for risk prediction and heritability estimation.

Results

Overview of methods

Our proposed method encompasses three steps. The overview of the method is outlined in **Fig. 1** and is described in detail in the Methods section.

In step 1, we fit a null linear or logistic mixed-effect model without genotypes to estimate the covariate effects. This step involves fitting the model using the average information restricted maximum likelihood (AI-REML)[24] approach, which is utilized in the SAIGE[25] and GMMAT[26] framework. Residuals will be used as covariate-adjusted phenotypes in the subsequent steps.

In step 2, we model the effect of rare variants (MAF $\leq$ 0.01) as random effects and estimate the variance components, and hence heritability. To mitigate the computational demands, we

adopt the Factored Spectrally Transformed Linear Mixed Models (FaST-LMM)[23]. Given $n \gg k$, FaST-LMM reduces the computation cost from $O(n^3)$ of conventional mixed model algorithm to $O(nk^2)$ where n is the number of samples in the dataset and k is the number of genetic variants in a single group (See **Methods**). Additionally, we leveraged the sparsity in genotypes. To incorporate the fact that genetic effects vary by functional annotations, we fit the model separately for distinct categories, and then combine them to calculate gene or region-level heritability. For whole exome analysis, we include three functional categories: (1) Loss-of-function (LoF) variants; (2) missense variants; and (3) synonymous variants. Within each category, the ultra-rare variants, defined as those with a minor allele count (MAC) of lower than 10, are collapsed into a single variant, as employed in SAIGE-GENE+[16]. As estimating multiple variance components due to distinct functional groups is not feasible with FaST-LMM, we marginally calculate variance component for each functional group separately, and then adjust them using method of moments (MoM) approach (See **Methods**).

In step 3, following the estimation of variance components, we calculate the effect size of each variant using the Best Linear Unbiased Predictor (BLUP) estimates[27-30]. We further estimate the prediction error variance (PEV) of the effect size estimates to assess the reliability of the variant-level effect sizes. For binary traits, we implemented Firth bias correction[31] as a subsequent step. This correction mechanism mitigates bias and rectifies abnormal estimates, especially in scenarios where the case-control ratio is imbalanced. Recognizing the imperative of scalability in large-scale biobank data analyses, we developed a fast implementation of Firth correction, which reduces computation complexity from $O(Mnk_F)$ to $O(n_{nz}k_F)$ where M is the average number of iterations for convergence of Firth corrected beta, n_{nz} is the number of individuals with non-zero genotype, and k_F denotes the number of variants that needs to be corrected (See **Methods**).

UK Biobank WES data analysis

We applied our method to 100 traits in the UKB, including clinically important quantitative traits such as cholesterol levels and major diseases such as type 2 diabetes and various cancers. The full list of analyzed traits is provided in **Supplementary Table 1**. For LDL cholesterol (LDL-C) level, we adjusted the pre-medication levels by dividing the raw LDL-C level by 0.7 for individuals on cholesterol-lowering medication[32].

We computed gene-level effect sizes by leveraging the estimated heritability derived from the mixed effects model. Recognizing the inherent unsigned nature of heritability, we assign a sign by incorporating variant-level effect sizes of loss-of-function (LoF) variants within each gene. This allows us to discern the direction of the effect of the gene on the trait (See **Methods**). As expected, the gene-based association test p-values and the magnitude of the gene-level effect size showed a substantial correlation (**Fig. 2** and **Supplementary Figure 1**). Incorporating gene-level effect size and direction on top of the gene-based association tests can add significant value to genetic analyses. For example, the signed heritability clearly shows that the impairment of APOC3 function increases HDL cholesterol (HDL-C) level but decreases triglycerides (**Fig. 2(a)** and **2(c)**).

We estimated the variant-level effect sizes of exonic variants and presented two genes, *APOC3* and *SLC12A3,* on HDL-C levels as examples (**Fig. 3**). As expected, variants demonstrating significant associations, in terms of p-values, also exhibited larger effect sizes. Using RareEffect, we observed that the majority of variants in *APOC3* displayed positive effect sizes. The Burden and SKAT-O p-values from SAIGE-GENE+ were both highly significant (Burden p-value = 1×10^{-298} and SKAT-O p-value = 1×10^{-300}). In contrast, variants in *SLC12A3* exhibited both positive and negative effect sizes. Consequently, Burden p-value was not significant (Burden p-value = 0.01), but the SKAT-O p-value was significant (SKAT-O p-value = 7×10^{-12}). This distinction in the directionality of effect sizes cannot be discerned through the burden approach.

We extended our analyses to estimate polygenic risk scores using rare variants with effect sizes estimated from RareEffect (PRS_{RE}). The UK Biobank data were randomly split into training and test sets (ratio = 8:2), and PRS_{RE} was constructed using the genes with p-values < 2.5×10^{-6} from SAIGE-GENE+ in the training set (See **Methods**). We included top 10 genes when the number of genes with p-values < 2.5×10^{-6} is smaller than 10. We further integrated these PRS_{RE} with PRS derived from common variants (PRS_{common}) using SBayesRC[33] to evaluate the practical utility of our approach. When combining the PRS from common and rare variants, we constructed a composite score, a linear combination of PRS from common and rare variants. We evaluated the predictive performance in terms of R^2.

Our RareEffect PRS (PRS_{RE}) showed higher R^2 for 97% of tested quantitative traits than PRS_{burden}, a comparative approach that relied on per-allele effect sizes derived from burden tests (**Fig. 4**, **Supplementary Table 2-4**, and **Supplementary Figure 2**). In addition, combining the common variant PRS with the PRS_{RE} to construct a composite score improved prediction performance in a number of phenotypes (**Supplementary Note A** and **Supplementary Table 2**). The improvement became pronounced for lipid phenotypes among individuals deemed at high risk. For instance, when predicting HDL and LDL cholesterol levels, PRS_{RE} achieved R^2 of 0.4737 and 0.6174 when restricting individuals with top/bottom 0.5% in terms of PRS_{RE}. When the composite score was used for risk prediction, R^2 were 0.6619 and 0.7012 when restricted to top/bottom 0.5% individuals. In contrast, common variants only PRS model had lower R^2 (0.6028 for HDL and 0.6046 for LDL) for top/bottom 0.5% individuals. Notably, the sub-groups identified as high-risk by PRS_{common} and PRS_{RE} were substantially distinct (**Supplementary Figure 3**), underscoring the complementary nature of rare variants in detecting individuals at elevated disease risk. Additionally, we observed that our model showed higher predictability compared to the Burden approach which showed R^2 of 0.3684 and 0.2362 for HDL and LDL with top/bottom 0.5% in terms of PRS using burden score (PRS_{burden}), respectively. We observed the similar pattern when PRS-CS[34] was used for PRS_{common} (**Supplementary Table 2**).

Our method exhibited marginally lower predictive performance for binary traits, as measured by enrichment of cases among high-risk groups and AUC, compared to the burden approach. We observed that for chosen binary traits, there were fewer genes associated with the trait, and their signals appeared weaker when contrasted with tested continuous traits. Nonetheless, our method offers potential benefits, as it can enhance predictability by combining PRS_{RE} with PRS_{common} and PRS_{burden}, which yielded better results. (**Supplementary Table 3, 4** and **Supplementary Note A**).

To further evaluate the utility of RareEffect, we compared its performance against other recent rare variant PRS methods incorporating functional annotations, including PrimateAI-3D, AlphaMissense, and DeepRVAT (**Supplementary Note B**). Across five phenotypes tested, RareEffect consistently demonstrated higher predictive accuracy, both as a standalone rare

178 variant PRS and when combined with common variant PRS. For instance, in the case of LDL
179 cholesterol, RareEffect achieved an R^2 of 0.0340, more than twice that of the other methods.
180 Moreover, when evaluating prediction performance in individuals at the extremes of the PRS
181 distribution (top/bottom 0.5%), RareEffect yielded the highest improvement in composite
182 score accuracy, with an R^2 gain of 0.1066, which is four times larger than the next best
183 approach PrimateAI-3D (R^2 gain 0.0273) (**Supplementary Table 5** and **Supplementary Figure**
184 **4, 5**).
185
186 We further examined the relationship between phenotype outliers and the PRS in identifying
187 individuals at high risk for common diseases[18]. We first defined the phenotype outliers as
188 individuals with phenotype value exceeding a certain z-score cutoff and calculated the
189 proportion of individuals with high PRS among phenotype outliers. Specifically, for LDL
190 cholesterol levels, PRS_{RE} successfully pinpointed individuals at phenotypic extremes, who
191 exhibited a tenfold higher likelihood of possessing a PRS_{RE} falling within 0.1st percentile
192 compared to the baseline population (**Supplementary Figure 6**). PRS_{RE} and PRS_{common}
193 utilize distinct set of variants and show minimal correlation (**Supplementary Table 6**).
194 Therefore, integrating these models into a unified framework enables the identification of a
195 significantly larger cohort at high risk than achievable through PRS_{common} alone.
196
197 *Simulation study*
198 To assess the estimation accuracy of our method, we conducted extensive simulations under
199 diverse scenarios (see **Methods**) for both binary and quantitative traits. To mimic real data,
200 we utilized actual genotypes from the UKB dataset, specifically the array-genotyped data for
201 common variants (MAF≥0.01) and the UKB WES data for rare variants (MAF≤0.01).
202
203 We compared the performance of variant-level effect size estimation from our method against
204 other existing approaches such as linear regression, which is used for standard single-variant
205 association test, or ridge regression using multiple evaluation metrics, including bias, mean
206 absolute error (MAE), root mean squared error (RMSE), and coverage rate. For quantitative
207 traits, our method consistently demonstrated a lower RMSE of 0.2101 on average,
208 outperforming the comparative methods which showed RMSE of 0.2271 (ridge regression) to

209 0.2228 (linear regression) (**Supplementary Table 7, 8**) when estimating the effect size. For
210 binary traits, our method also exhibited lower estimation error particularly in scenarios of low
211 disease prevalence compared to ridge regression (**Supplementary Table 9**). Conversely, ridge
212 regression showed marginally reduced RMSE compared to our method in instances of high
213 disease prevalence; however, the difference in estimation accuracy remains modest.
214
215 To evaluate the prediction performance, we compared true $G_{rare}\beta$ of simulated data and
216 predicted $G_{rare}\hat{\beta}$, where G_{rare} include all rare variants across 50 causal genes. The results
217 showed that RareEffect achieved lower MAE and RMSE on average compared to the
218 comparative methods (**Supplementary Table 10**). We note that RareEffect, similar to Ridge
219 regression, exhibited a higher calibration slope, reflecting the inherent shrinkage of the
220 method. However, because polygenic risk score (PRS) models are typically subjected to model
221 calibration prior to application, we emulated this by calibrating the slope using a subset of
222 samples via regression model. As expected, after regression calibration, all methods achieved
223 a calibration slope of approximately 1.
224
225 We also evaluated the performance of RareEffect on the estimation of gene-level heritability
226 comparing with RARity[35], which uses adjusted R^2 (**Supplementary Note CE**). Our analysis
227 shows that RareEffect tends to perform better when the true heritability is small and less
228 biased than RARity, but RARity can perform better when true heritability is high
229 (**Supplementary Table 11**). Additional analysis of different sample sizes showed that
230 RareEffect stably estimate heritability with sample size > 100,000 (**Supplementary Table 12**).
231
232 *Computation and memory cost*
233 Analyzing 166,960 samples from the UKB WES data to estimate the effect size of the *DOCK6*
234 gene, which contains 4,114 rare variants, we observed that the computation time for
235 RareEffect with a simulated phenotype was approximately 90% lower than that of ridge
236 regression. Specifically, RareEffect completed the analysis in 4.2 seconds, compared to 44.6
237 seconds for ridge regression (**Supplementary Figure 7).** The memory usage for RareEffect
238 during the analysis was 1.14GB for *DOCK6* gene (**Supplementary Figure 8**). For binary traits,
239 an additional step of performing Firth bias correction is required. We observed that the
240 normal Firth bias correction process took 708 seconds to analyze a gene with 250 variants

241 (after collapsing) across 342,409 individuals. However, by implementing our fast version of
242 Firth correction, the computation time was dramatically reduced to 2.9 seconds
243 (**Supplementary Figure 9**).
244
245 **Discussion**
246 Our study introduces a novel method aimed at estimating the effect size of rare variants and
247 can be extended to estimate gene-level effect size by employing a two-stage framework of
248 generalized linear mixed models. By leveraging the variant-level effect size estimates obtained
249 through our approach, we can examine the collective impact of rare variants within a gene
250 and quantify their contribution to the overall heritability of complex traits.
251
252 In order to obtain accurate estimates for effect sizes while optimizing computational efficiency,
253 we employed several techniques in our analysis. First, we utilized the FaST-LMM[23] algorithm
254 to expedite computation and reduce memory usage. Unlike GWAS settings where FaST-LMM
255 relies on subsampling variants to reduce rank of genetic relatedness matrix, RareEffect
256 operates in a regime where the number of variants per gene (k) is inherently much smaller
257 than the sample size (n). This allows us to apply the FaST-LMM algorithm without
258 approximation, reducing the time complexity while retaining exact computation. Second, we
259 implemented the optimized version of Firth bias correction by utilizing the sparsity of
260 genotype matrix and skipping the computation of hat matrix at every iteration. Third, we
261 employed a collapsing strategy that reduces the sparsity of the data, similar to the approach
262 employed in SAIGE-GENE+. These algorithmic approaches accelerate the estimation process
263 and enhance computational scalability, particularly when dealing with large-scale datasets.
264
265 Prediction error variance (PEV) estimated in our method can be used to calculate confidence
266 intervals. However, because RareEffect employs a shrinkage-based approach, and confidence
267 intervals constructed using these estimates may not reliably cover the true effect sizes. In
268 particular, we observed that the coverage rate for true causal variants was generally low,
269 which reflects a known limitation of shrinkage estimators[36-38]. Nonetheless, for null variants,
270 the confidence intervals consistently captured zero (**Supplementary Table 7**), indicating that
271 the method accurately identifies non-causal variants. Furthermore, among the cases where
272 the confidence intervals failed to cover the effect size of true causal variant, more than 99.999%

of the intervals were positioned closer to zero than the true beta value, suggesting that these failures tend to occur in a conservative direction (**Supplementary Table 13**). Therefore, although the overall coverage rate is reduced, this does not appear to increase type I error but rather reflects a conservative bias in the effect size estimation. Among the methods compared, multiple linear regression exhibited lower coverage for null variants, suggesting potential inflation of type I error rates. Additionally, since variant-level effect size estimation involves multiple statistical tests, multiplicity adjustment may be necessary. Standard approaches such as Bonferroni adjustment[39] or false discovery rate (FDR) control[40] can be applied, and multiplicity-corrected confidence intervals for odds ratios[41] can also be considered.

To assess genetic differences by sex, we compared estimated gene-level heritability between genetic sexes for three lipid traits (HDL, LDL and TG) (**Supplementary Note D). Supplementary Table 14** shows estimated heritability for top 10 genes. Overall, the estimated heritabilities are generally consistent with very high Pearson correlation.

In principle, the framework of RareEffect can be extended to other variant types such as copy number variants (CNVs) and intergenic variants, provided appropriate grouping strategies are defined. For intergenic variants or CNVs, the key challenge lies in defining biologically meaningful groups—such as proximity to regulatory elements or shared structural features—after which RareEffect's variance component modeling can be applied.

Beyond its immediate applications in effect size estimation, our proposed method can enhance polygenic risk prediction models. Traditionally, these models have relied on common variants. Our analysis reveals that the correlation between PRS_{RE} and phenotype values in the general population is not substantial (**Supplementary Figure 10**), so can provide complementary information.

AI-based methods[22,42] have been developed to enhance the pathogenicity prediction of rare variants. Although these approaches can help to identify effect sizes of pathogenic variants and can be used for risk prediction, they may not be as effective for identifying beneficial or gain-of-function variants. As shown in our study, these methods have substantially low

305 predictive performance than RareEffect. Additionally, the performance of these methods can
306 be limited when applied to non-protein-altering variants. Our approach can accommodate the
307 predictively pathogenic variants identified by AI-based models by forming them into a
308 separate category, thereby enhancing performance.
309
310 RareEffect uses the MoM estimator to account for LD within a gene when estimating variance
311 components. While this approach effectively adjusts for LD in most cases, it presents a
312 challenge when the overall genetic effect of a gene is small. In such cases, the MoM estimator
313 can produce negative variance component estimates, making the adjustment infeasible
314 (**Supplementary Table 15**). When this occurs, the unadjusted marginal variance component
315 estimates need to be used, which can lead to a slight overestimation of gene-level heritability.
316 Although this issue is relatively infrequent and primarily affects genes with minimal
317 contribution to heritability, it remains an important consideration when interpreting results.
318
319 We note that RareEffect is specifically designed to estimate gene-level heritability rather than
320 exome-wide heritability. Estimating exome-wide heritability would require aggregating gene-
321 level heritability estimates across all genes, but doing so involves additional assumptions. For
322 instance, RARity conducted extensive pruning to adjust for long-range LD. Similar approach
323 should be used to apply RareEffect to estimate exome-wide heritability.
324
325 In our study, gene-level effect directions were estimated using MAF-weighted effect sizes of
326 predicted loss-of-function (LoF) variants. This approach performed well in both simulation
327 studies and real data analyses, yielding results concordant with the true effect directions in
328 simulations and with burden test results in real data (**Supplementary Note E**). The method
329 assumes that predicted LoF variants within a gene have consistent effect directions. While this
330 assumption would generally hold, exceptions may arise due to true biological heterogeneity
331 or misclassification of functional impact. In such cases, discrepancies between the estimated
332 and true gene-level effect directions may occur, potentially influencing downstream analyses.
333
334 Our study has several limitations. While RareEffect demonstrates comparable or superior
335 performance in estimating the effect size for simulated binary phenotypes, our evaluation
336 revealed only marginal enhancements in predictive performance, compared to the common

variant PRS, across tested disease phenotypes, and these improvements were generally not statistically significant (**Supplementary Table 16**). This could be attributed to the trait's reliance on a limited number of ultra-rare variants, which our method collapses into super-variants, thereby complicating the estimation of variant-level effect sizes for true causal variants. In addition, the binary phenotypes analyzed in this study generally had a much smaller number of significantly associated genes, which likely limited the potential benefit from rare variant PRS in these traits. Despite its efficacy in effect size estimation, RareEffect's ability to improve prediction accuracy remains constrained, highlighting a potential area for future refinement and investigation for risk prediction of binary traits. Additionally, it is important to note that RareEffect is based on BLUP estimate, characterized by shrinkage properties, leading to biased estimates of effect sizes. To reduce bias, we also have implemented adaptive ridge for L0-regularization approach[43] in the top of BLUP estimation. (**Supplementary Note F**). Adaptive Ridge provided improvement in bias (**Supplementary Table 7),** but phenotype prediction was not improved. Further investigation is warranted and left for future work.

In summary, our results demonstrate that incorporating information from rare variants enables the accurate estimation of gene-level and variant-level effect sizes, as well as the identification of high-risk individuals who might remain undetected by conventional polygenic risk scores (PRS) methods relying on common variants.

Methods

Generalized linear mixed model

We denote the phenotype of the ith individual using y_i for both quantitative and binary traits in a study with sample size n. $\boldsymbol{X}$ represents the $n \times (p+1)$ vector with p covariates including the intercept, and $\boldsymbol{G}_j$ is the $n \times k$ matrix representing the minor allele counts for k rare variants in gene or region j. The generalized linear mixed model (GLMM) can be expressed as:

$$g(\boldsymbol{\mu}) = \boldsymbol{X\alpha} + \boldsymbol{G}_j\boldsymbol{\beta}_j + \boldsymbol{b}$$

where $\boldsymbol{\mu}$ is the mean phenotype, $\boldsymbol{b} \sim MVN(0, \sigma_g^2\boldsymbol{K})$ is the random effect, and $\boldsymbol{K}$ is an $n \times n$ genetic relatedness matrix (GRM). And g is the link function which is an identity function for quantitative traits with error term $\boldsymbol{\epsilon} \sim MVN(0, \sigma_e^2\boldsymbol{I}_n)$ and a logit function for binary traits. The

parameter $\boldsymbol{\alpha}$ is a $(p+1) \times 1$ vector of fixed effect coefficients and $\boldsymbol{\beta}_j$ is a $k \times 1$ vector of the random genetic effect.

Fitting the null generalized mixed model (step 1)

We used the average information restricted maximum likelihood (AI-REML) algorithm to fit the null GLMM (i.e., H_0: $\boldsymbol{\beta}_j = \mathbf{0}$) as in SAIGE step 1.

Estimation of the gene-level (region-level) heritability (step 2)

We estimate the effect size of rare variants using the following linear mixed model:

$$\tilde{\boldsymbol{y}} = \boldsymbol{G}_j \boldsymbol{\beta}_j + \boldsymbol{\epsilon}$$

where $\tilde{\boldsymbol{y}} = (\tilde{y}_1, \dots, \tilde{y}_n)^T = \boldsymbol{y} - \hat{\boldsymbol{y}}$ for quantitative traits, $\tilde{y}_i = \frac{d\eta_i}{d\mu_i}(y_i - \hat{\mu}_i) = \frac{1}{\hat{\mu}_i(1-\hat{\mu}_i)}(y_i - \hat{\mu}_i)$, a working residual from iteratively reweighted least squares (IRWLS) for binary traits, and $\hat{\mu}_i$ is the mean phenotype for individual i, which can be obtained from step 1. When obtaining $\boldsymbol{G}_j$, as in SAIGE-GENE+, we collapsed ultra-rare variants with minor allele count (MAC) ≤ 10 by each gene and functional group to reduce the sparsity. We further implemented an option to collapse all loss-of-function (LoF) rare variants into a single column[44], irrespective of their minor allele count, adopting the burden approach. This approach is predicated on the assumption that all rare LoF variants share a common effect size and direction. For binary traits, when we use working residuals, the variance of $\tilde{y}_i$ differs by individual, so we cannot apply the optimization technique of FaST-LMM. Therefore, we divide both sides by the square root of variance of $\tilde{y}_i$ to make the variance be the same across individuals. We estimate the effect size using the modified model, for binary traits:

$$\hat{\boldsymbol{\Sigma}}_\epsilon^{-\frac{1}{2}} \tilde{\boldsymbol{y}} = \hat{\boldsymbol{\Sigma}}_\epsilon^{-\frac{1}{2}} \boldsymbol{G}_j \boldsymbol{\beta}_j + \hat{\boldsymbol{\Sigma}}_\epsilon^{-\frac{1}{2}} \boldsymbol{\epsilon}$$

where $\hat{\boldsymbol{\Sigma}}_\epsilon = \mathrm{diag}(\frac{1}{\hat{\mu}_i(1-\hat{\mu}_i)})$.

In this model, the prior distribution of $\boldsymbol{\beta}_j$ are assumed to follow $MVN(0, \tau\boldsymbol{\Sigma})$, and the noise $\boldsymbol{\epsilon}$ is assumed to follow $MVN(0, \psi \boldsymbol{I}_n)$ for quantitative traits, while we assume $\hat{\boldsymbol{\Sigma}}_\epsilon^{-\frac{1}{2}} \boldsymbol{\epsilon}$ follows $MVN(0, \psi \boldsymbol{I}_n)$ for binary traits. When there is no prior knowledge of the correlation within $\boldsymbol{\beta}$, $\boldsymbol{\Sigma}$ is set to be an identity matrix. But in general, $\boldsymbol{\Sigma}$ does not have to be an identity or a diagonal matrix.

To estimate the variance component parameters (τ, ψ), we use factored spectrally transformed linear mixed models (FaST-LMM) algorithm. Let $\widetilde{\boldsymbol{G}} = [\widetilde{\boldsymbol{G}}_1, \dots, \widetilde{\boldsymbol{G}}_k]$ be an $n \times k$ genotype matrix of the region with $\widetilde{\boldsymbol{G}}_j = \boldsymbol{G}_j$ for quantitative traits and $\widetilde{\boldsymbol{G}}_j = \widehat{\boldsymbol{\Sigma}}_\epsilon^{-\frac{1}{2}} \boldsymbol{G}_j$ for binary traits. The variance of $\widetilde{\boldsymbol{y}}$ (quantitative traits) or $\widehat{\boldsymbol{\Sigma}}_\epsilon^{-\frac{1}{2}} \widetilde{\boldsymbol{y}}$ (binary traits) can be written as

$$\boldsymbol{\tau} \widetilde{\boldsymbol{G}} \boldsymbol{\Sigma} \widetilde{\boldsymbol{G}}^T + \psi \boldsymbol{I}_n$$

Traditional approaches to estimate the variance components require either calculating inverse matrix or conducting spectral decomposition of the $n \times n$ matrix $\widetilde{\boldsymbol{G}} \boldsymbol{\Sigma} \widetilde{\boldsymbol{G}}^T$, so the time complexity is of $O(n^3)$. In contrast, FaST-LMM algorithm uses the fact that $\widetilde{\boldsymbol{G}} \boldsymbol{\Sigma} \widetilde{\boldsymbol{G}}^T$ has rank at most k, so to reduce the computation complexity. Suppose $\boldsymbol{Z} = \widetilde{\boldsymbol{G}} \boldsymbol{L}$ is an $n \times k$ matrix where $\boldsymbol{L}$ is a Cholesky factor of $\boldsymbol{\Sigma}$. Then $\widetilde{\boldsymbol{G}} \boldsymbol{\Sigma} \widetilde{\boldsymbol{G}}^T = \boldsymbol{Z} \boldsymbol{Z}^T$. FaST-LMM carries out singular value decomposition on $\boldsymbol{Z}$ and calculate likelihood for (τ, ψ). With given $n \gg k$, calculation of $\boldsymbol{Z}$ and its singular value decomposition requires only $O(nk^2)$ of time complexity. And we further improved the computation efficiency utilizing the sparsity of $\boldsymbol{Z}$[45]. In biobank-scale data, n is in the hundreds of thousands, and k is in the tens to hundreds on average which means $n \gg k$.

Using the above optimization technique, we estimate the variance components by each group. Consider one group (LoF, missense or synonymous) in a single gene j in the model:

$$\widetilde{\boldsymbol{y}} = \boldsymbol{G}_{\cdot,j} \boldsymbol{\beta}_{\cdot,j} + \boldsymbol{\epsilon}$$

We first marginally estimate the maximum-likelihood estimator (MLE) of variance components $\tau_{LoF,j}$, $\tau_{mis,j}$, and $\tau_{syn,j}$. As the marginal estimates do not account for LD among variants in different groups, we adjust the estimates using method of moments (MoM) approaches[46]. The MoM estimator can be obtained by solving the following linear system:

$$\begin{bmatrix} \boldsymbol{T} & \boldsymbol{b} \\ \boldsymbol{b}^T & n \end{bmatrix} \begin{bmatrix} \hat{\boldsymbol{\tau}} \\ \hat{\psi} \end{bmatrix} = \begin{bmatrix} \boldsymbol{c} \\ \widetilde{\boldsymbol{y}}^T \widetilde{\boldsymbol{y}} \end{bmatrix}$$

where $\boldsymbol{T}$ is a 3×3 matrix for joint estimation or a scalar (1×1 matrix) for marginal estimation with entries $\boldsymbol{T}_{k,l} = \mathrm{tr}(\widetilde{\boldsymbol{G}}_k \boldsymbol{\Sigma}_k \widetilde{\boldsymbol{G}}_k^T \widetilde{\boldsymbol{G}}_l \boldsymbol{\Sigma}_l \widetilde{\boldsymbol{G}}_l^T)$ where $k, l \in \{1, 2, 3\}$ for joint estimation. $\boldsymbol{b}$ is a 3-vector for joint estimation or a scalar for marginal estimation with entries $b_k = \mathrm{tr}(\widetilde{\boldsymbol{G}}_k \boldsymbol{\Sigma}_k \widetilde{\boldsymbol{G}}_k^T)$, $\boldsymbol{c}$ is a 3-vector for joint estimation or a scalar for marginal estimation with entries

$c_k = \widetilde{\boldsymbol{y}}^T \widetilde{\boldsymbol{G}}_k \boldsymbol{\Sigma}_k \widetilde{\boldsymbol{G}}_k^T \widetilde{\boldsymbol{y}}$, and $\hat{\boldsymbol{\tau}} = \begin{bmatrix} \widehat{\tau_1} \\ \widehat{\tau_2} \\ \widehat{\tau_3} \end{bmatrix}$ where (τ_1, τ_2, τ_3) denotes $(\tau_{LoF,j}, \tau_{mis,j}, \tau_{syn,j})$ for a single gene j, respectively.

After estimating the marginal and joint MoM estimator of variance components, we adjust the MLE of the marginal variance components by:

$$\hat{\tau}_{i,j} = \hat{\tau}_{MLE,mar,i,j} \times \frac{\hat{\tau}_{MoM,joint,i,j}}{\hat{\tau}_{MoM,mar,i,j}}$$

where $i \in \{LoF, mis, syn\}$. The MoM estimator of the variance component was not directly utilized in our study since the MoM estimator could yield negative variance components. In cases of the variance component estimated by the MoM is negative, we used marginal variance component without adjustment. Both MoM and likelihood-based approaches exhibited the similar trends of variance components (**Supplementary Figure 11**). Additionally, we assume that the variance explained by rare variants in a single gene is negligibly small[35] compared to the total variance of $\tilde{y}$, therefore, $\hat{\psi} \approx Var(\tilde{y})$.

We estimated the heritability from rare variants of gene j using these adjusted variance components. In a joint model,

$$Var(\widetilde{\boldsymbol{y}}) = \boldsymbol{G}_j \boldsymbol{\Sigma}_j \boldsymbol{G}_j^T + \psi \boldsymbol{I}_n$$

where $\boldsymbol{G}_j = [\boldsymbol{G}_{LoF,j} \quad \boldsymbol{G}_{mis,j} \quad \boldsymbol{G}_{syn,j}]$ and $\boldsymbol{\Sigma}_j = \begin{bmatrix} \hat{\tau}_{LoF,j}\boldsymbol{\Sigma}_{LoF,j} & \boldsymbol{0} & \boldsymbol{0} \\ \boldsymbol{0} & \hat{\tau}_{mis,j}\boldsymbol{\Sigma}_{mis,j} & \boldsymbol{0} \\ \boldsymbol{0} & \boldsymbol{0} & \hat{\tau}_{syn,j}\boldsymbol{\Sigma}_{syn,j} \end{bmatrix}$.

Therefore,

$$\sum_{i=1}^{n} Var(\widetilde{y}_i) = \mathrm{tr}(\boldsymbol{G}_j \boldsymbol{\Sigma}_j \boldsymbol{G}_j^T) + n\psi \quad \text{(for quantitative traits)}$$

$$\sum_{i=1}^{n} Var(\widetilde{y}_i) = \mathrm{tr}(\boldsymbol{G}_j \boldsymbol{\Sigma}_j \boldsymbol{G}_j^T) + n\,\mathrm{tr}(\widehat{\boldsymbol{\Sigma}}_\epsilon) \quad \text{(for binary traits)}$$

Subsequently, the heritability from rare variants of gene j can be denoted as:

$$h_j^2 = \frac{\mathrm{tr}\left(\boldsymbol{G}_j \boldsymbol{\Sigma}_j \boldsymbol{G}_j^T\right)}{\mathrm{tr}\left(\boldsymbol{G}_j \boldsymbol{\Sigma}_j \boldsymbol{G}_j^T\right) + n\psi} \quad \text{(for quantitative traits)}$$

$$h_j^2 = \frac{\mathrm{tr}\left(\boldsymbol{G}_j \boldsymbol{\Sigma}_j \boldsymbol{G}_j^T\right)}{\mathrm{tr}\left(\boldsymbol{G}_j \boldsymbol{\Sigma}_j \boldsymbol{G}_j^T\right) + \psi\,\mathrm{tr}(\widehat{\boldsymbol{\Sigma}}_\epsilon)} \quad \text{(for binary traits)}$$

Additionally, to determine the direction of the gene-level effect, we obtained the sign of the linear combination of the effect sizes of loss-of-function variants in a gene, weighted by their MAFs:

$$\text{(signed heritability of gene } j) = h_j^2 \times \mathrm{sgn}(\textstyle\sum_{j \in LoF} \beta_j \, MAF_j)$$

This measure gives the information of the magnitude of genetic effects from rare variants in a single gene and its direction of effects.

Estimation of the variant-level effect size (step 3)

The effect sizes at variant-level resolution are estimated using the adjusted variance components in the previous step by:

$$\widehat{\boldsymbol{\beta}}_j = \left(\widetilde{\boldsymbol{G}}_j^T \widetilde{\boldsymbol{G}}_j + \hat{\psi} \boldsymbol{\Sigma}_j^{-1}\right)^{-1} \widetilde{\boldsymbol{G}}_j^T \widetilde{\boldsymbol{y}}$$

for each gene or region.

We further estimated the prediction error variance (PEV) by:

$$PEV(\widehat{\boldsymbol{\beta}}_j) = \left(\widetilde{\boldsymbol{G}}_j^T \widetilde{\boldsymbol{G}}_j + \frac{\hat{\psi}}{\hat{\tau}} \boldsymbol{I}\right)^{-1}$$

for each gene or region. Using this PEV, we can obtain confidence intervals for effect sizes.

For binary traits, the Firth bias correction[31] is a more accurate method to estimate SNP effect sizes[47-49], particularly in cases marked by a significant case-control imbalance. We incorporate this correction into our analytical framework. Additionally, we introduce an L2 penalty term to account for the prior distribution of $\boldsymbol{\beta}$. The Firth corrected effect estimates can be calculated numerically by optimizing the following objective function:

$$\hat{\beta}_* = \mathrm{argmax}_\beta [\log L(\beta) + \frac{1}{2} \log |I(\beta)| - \frac{1}{2\hat{\tau}} \|\beta\|_2^2]$$

where L denotes the likelihood function and I is the Fisher information.

To improve computational efficiency, we developed the fast implementation of Firth bias correction. First, we compute the hat matrix, $\boldsymbol{H} = \boldsymbol{W}^{\frac{1}{2}} \boldsymbol{X} (\boldsymbol{X}^T \boldsymbol{W} \boldsymbol{X})^{-1} \boldsymbol{X}^T \boldsymbol{W}^{\frac{1}{2}}$, $\boldsymbol{W} = \mathrm{diag}(\widehat{\mu}_i (1 - \widehat{\mu}_i))$, only once rather than recalculating it at each iteration, assuming that the iterative weights ($\boldsymbol{W}$) change slowly as a function of the mean μ_i[26,50]. We compared, using both simulation and real data, the difference in effect size estimates between computing the hat

matrix once and computing it at each iteration. Our findings indicate minimal differences in the effect size estimates (**Supplementary Figure 12**). Given that Firth correction is applied to each variant, we iterate the hat matrix calculation for k_F times, where k_F represents the number of variants that need to be corrected. This strategy results in a reduction in the computational complexity with Firth correction from $O(Mnk_F)$ to $O(nk_F)$, where M is the average number of iterations needed for Firth corrected effect size convergence. Second, we extend Firth correction to accommodate sparse genotype matrices. Specifically, we restrict our computations to individuals with non-zero genotypes when determining the score and Fisher information. This further reduces the time complexity of the Firth correction, now at $O(n_{nz}k_F)$, where n_{nz} denotes the number of individuals with non-zero genotype. Considering that we are estimating the effect size of rare variants with MAF < 0.01, we observed that $n_{nz} < 0.01n$ which implies that leveraging sparsity makes the estimation of effect sizes more than 100 times faster compared to a non-sparse approach.

We note that Firth correction is used when the absolute value of estimated effect size ($\hat{\beta}$) surpasses a predefined threshold. In this study, we used threshold of $\log 2 \approx 0.693$ for simulation studies and real data analysis.

RareEffect utilizes a shrinkage-based framework for estimating variant-level effect sizes, which inherently introduces bias. To mitigate this limitation, we incorporated an optional extension based on an adaptive ridge approach that provides a computationally efficient approximation to L0-regularization (**Supplementary Note F**).

Rare-variant PRS calculation

We further calculated polygenic risk scores using the variant-level effect sizes of rare variants (PRS_{RE}) in genes with gene-level p-value from SAIGE-GENE+ lower than 2.5×10^{-6}. PRS_{RE} of individual i can be calculated as:

$$PRS_{RE,i} = \sum_{j \in J} \boldsymbol{G}_{ij} \widehat{\boldsymbol{\beta}}_j$$

where J denotes a set of genes with gene-level p-value lower than 2.5×10^{-6}. Additionally, we combined these PRS_{RE} with PRS_{common} only. We applied PRS-CS[34] and SBayesRC[33] to obtain the variant-level weights for the calculation the PRS_{common} . We compared the

predictive performance of the PRS_{RE} to PRS_{burden}. PRS_{burden} were obtained in two different ways: (1) collapsing rare variants by functionality of the variants (LoF, missense, and synonymous), which is labeled as "Burden 1" in Supplementary Table, and (2) collapsing all rare variants into one super-variant regardless of functionality, labeled as "Burden 2" in Supplementary Table. In general, Burden 1 exhibited superior predictive performance compared to Burden 2 across most cases. Therefore, we used Burden 1 as the baseline for comparison in our analysis. After collapsing, we fitted the following linear model to estimate the per-allele effect sizes:

$$\tilde{y} = \boldsymbol{G}_{burden,j}\boldsymbol{\beta}_{burden,j}$$

The burden PRS are also calculated as a linear combination of per-allele effect sizes and the collapsed genotypes of each individual.

We compared the predictive performance in terms of R^2 for quantitative traits, and the area under receiver operating characteristic curve (AUROC) for binary traits of the following linear models:

$$\tilde{y} \sim PRS_{composite}$$

$$\tilde{y} \sim PRS_{common} + PRS_{RE}$$

$$\tilde{y} \sim PRS_{common} + PRS_{burden}$$

where $PRS_{composite}$ is a linear combination of PRS_{common} and PRS_{RE} with weights trained from the training set.

Additionally, we compared the performance of several recent methods for calculating rare variant PRS, including DeepRVAT, AlphaMissense, PrimateAI-3D, and RareEffect (See **Supplementary Note B**)

UK Biobank data analysis

In this study, we used WES data of 393,247 White British participants in the UK Biobank. The UK Biobank is a UK-based prospective cohort of ~500,000 individuals aged 40 to 69 at enrollment. We split the train and test data 8:2 randomly for the PRS evaluation. We applied quality control (QC) procedures prior to the analysis. We first removed redundant samples and individuals with sex mismatch or sex chromosome aneuploidy. Additionally, we further removed variants with a missingness rate across individuals > 0.1, HWE p-value < 10^{-15}, and

545 monomorphic variants. We generated group files, which define the list of variants in genes
546 and its functional annotation, by using the loss-of-function transcript effect estimator
547 (LOFTEE)[51]. We regarded a variant as loss-of-function (LoF) only in case of it is labeled as a
548 high-confidence (HC) LoF variant, and variants with low-confidence (LC) were regarded as
549 missense variants.
550
551 Using the data after QC, we applied our method to five quantitative traits (HDL cholesterol,
552 LDL cholesterol, triglycerides, height, and body mass index) and five binary traits (breast
553 cancer, prostate cancer, lymphoid leukemia, type 2 diabetes, and coronary atherosclerosis).
554 We defined the disease by mapping ICD-10 codes to Phecodes using the PheWAS R package[52].
555
556 *Simulation study*
557 To generate outcome phenotypes, we used the following model for quantitative and binary
558 traits:
559 $$y_i = X_{i1} + X_{i2} + G_{i,common}\beta_{common} + G_{i,rare}\beta_{rare} + \epsilon$$
560 $$logit\big(P(Y_i = 1)\big) = \alpha + X_{i1} + X_{i2} + G_{i,common}\beta_{common} + G_{i,rare}\beta_{rare}$$
561 where X_{i1} and X_{i2} are covariates, and $G_{i,common}$ and $G_{i,rare}$ are genotype vectors of common
562 variants and rare variants of ith individual, respectively. The intercept α for binary traits is
563 determined by the disease prevalence. The covariates X_{i1} and X_{i2} were simulated from
564 Bernoulli(0.5) and $N(0,1)$, respectively. For common variant effect, we randomly selected
565 L =30,000 LD-pruned common variants with MAF > 1%, and assumed that the effect size of
566 single common variant follows $N(0,\frac{1}{L})$. We selected 50 causal genes in UKB WES 200k data for
567 generation of phenotypes.
568
569 We used eight different scenarios regarding rare variants: (1) proportion of causal variants, (2)
570 effect size of causal variants, and (3) direction of effect within a single gene. For the proportion
571 of causal variants, we assumed (1) 20% of LoF, 10% of missense, and 2% of synonymous
572 variants, or (2) 30% of LoF, 10% of missense, and 2% of synonymous variants among rare
573 variants that are not ultra-rare are causal. For ultra-rare variants, we assumed that the
574 proportion of causal variants are three times higher than the non-ultra-rare variants, that is,
575 (1) 60% of LoF, 30% of missense, and 6% of synonymous ultra-rare variants, or (2) 90% of LoF,

30% of missense, and 6% of synonymous ultra-rare variants are causal. Regarding the effect size of causal variants, we assumed that the absolute effect sizes of causal variants are (1) $|0.5 \log_{10} MAF|$ for LoF variants, and $|0.25\log_{10} MAF|$ for missense and synonymous variants, or (2) $|0.3 \log_{10} MAF|$ for LoF variants, and $|0.15\log_{10} MAF|$ for missense and synonymous variants. We further assumed that the effect directions are (1) the same among all causal variants in a single gene, or (2) same for 100% of LoF, 80% of missense, and 50% of synonymous variants, while remaining variants have the opposite direction of effect. For eight combinations of scenarios, we repeated the simulation for 1,000 times. To evaluate the prediction performance, we calculated $G_{rare}\beta_{rare}$ and predicted $G_{rare}\hat{\beta}_{rare}$. Additional model calibration was conducted using a linear regression model of $G_{rare}\beta_{rare}$ and $G_{rare}\hat{\beta}_{rare}$ using 10% of simulated samples.

Computation cost evaluation

We evaluated the computation time and memory usage using simulated data as described above, comprising 166,960 individuals of White British ancestry from the UKB WES 200k dataset. Additionally, we examined computation time and memory usage across subsets with sample sizes of 10k, 30k, 50k, and 100k. For each generative scenario, we reported the mean of 5 attempts for computation times and memory usage, comparing them with multiple linear regression, simple linear regression (as in GWAS), and ridge regression. The evaluation for linear regression and ridge regression was done using lm and glm functions in R, respectively.

Data availability

The analysis results for 100 phenotypes of UKB WES data analysis results are available at: https://storage.googleapis.com/leelabsg/RareEffect/RareEffect_effect_size.zip (variant-level effect size) and https://storage.googleapis.com/leelabsg/RareEffect/RareEffect_h2.zip (gene-level signed heritability).

URLs

SAIGE (including SAIGE-GENE+): https://github.com/saigegit/SAIGE

DeepRVAT: https://github.com/PMBio/deeprvat

AlphaMissense scores: https://zenodo.org/records/8208688

PrimateAI-3D scores: https://primateai3d.basespace.illumina.com/

SBayesRC (GCTB): https://cnsgenomics.com/software/gctb

PRS-CS: https://github.com/getian107/PRScs

RARity: https://github.com/GMELab/RARity

Code availability

RareEffect is implemented as a part of SAIGE software, which is an open-source R package, available at https://github.com/saigegit/SAIGE. RareEffect is available in SAIGE version 1.3.7 or higher.

Author Contribution

K.N. and S.L. designed experiments. K.N. performed experiments and analyzed the UKB WES data. K.N. and S.L. implemented the software with input from W.Z.. M.K. and B.M. provided helpful advice. K.N. and S.L. wrote the manuscript with input from all co-authors.

Acknowledgements

This research was supported by the Brain Pool Plus (BP+) Program through the National Research Foundation of Korea (NRF) funded by the Ministry of Science and ICT (2020H1D3A2A03100666) and the grants funded by the Ministry of Food and Drug Safety, Republic of Korea (Grant Number: 23212MFDS202). Minjung Kho was supported by the NRF grant funded by the Korean government (MSIT) (NRF-2022R1C1C2006474). This research was conducted using the UK Biobank Resource under application number 45227.

References

1. Bycroft, C. *et al.* The UK Biobank resource with deep phenotyping and genomic data. *Nature* **562**, 203-209 (2018).
2. Gibson, G. Rare and common variants: twenty arguments. *Nat Rev Genet* **13**, 135-45 (2012).
3. Kryukov, G.V., Shpunt, A., Stamatoyannopoulos, J.A. & Sunyaev, S.R. Power of deep, all-exon resequencing for discovery of human trait genes. *Proc Natl Acad Sci U S A* **106**, 3871-6 (2009).
4. MacArthur, D.G. *et al.* A systematic survey of loss-of-function variants in human protein-coding genes. *Science* **335**, 823-8 (2012).
5. Genomes Project, C. *et al.* An integrated map of genetic variation from 1,092 human genomes. *Nature* **491**, 56-65 (2012).
6. Rivas, M.A. *et al.* Deep resequencing of GWAS loci identifies independent rare variants associated with inflammatory bowel disease. *Nat Genet* **43**, 1066-73 (2011).
7. Saint Pierre, A. & Génin, E. How important are rare variants in common disease? *Briefings in Functional Genomics* **13**, 353-361 (2014).
8. Perrone, F., Cacace, R., van der Zee, J. & Van Broeckhoven, C. Emerging genetic complexity and rare genetic variants in neurodegenerative brain diseases. *Genome Med* **13**, 59 (2021).
9. Manolio, T.A. *et al.* Finding the missing heritability of complex diseases. *Nature* **461**, 747-53 (2009).
10. Lee, S., Abecasis, G.R., Boehnke, M. & Lin, X. Rare-variant association analysis: study designs and statistical tests. *Am J Hum Genet* **95**, 5-23 (2014).
11. Chen, W., Coombes, B.J. & Larson, N.B. Recent advances and challenges of rare variant association analysis in the biobank sequencing era. *Front Genet* **13**, 1014947 (2022).
12. Wu, M.C. *et al.* Rare-variant association testing for sequencing data with the sequence kernel association test. *Am J Hum Genet* **89**, 82-93 (2011).
13. Lee, S. *et al.* Optimal unified approach for rare-variant association testing with application to small-sample case-control whole-exome sequencing studies. *Am J Hum Genet* **91**, 224-37 (2012).
14. Li, X. *et al.* Dynamic incorporation of multiple in silico functional annotations empowers rare variant association analysis of large whole-genome sequencing studies at scale. *Nat Genet* **52**, 969-983 (2020).
15. Zhou, W. *et al.* Scalable generalized linear mixed model for region-based association tests in large biobanks and cohorts. *Nat Genet* **52**, 634-639 (2020).
16. Zhou, W. *et al.* SAIGE-GENE+ improves the efficiency and accuracy of set-based rare variant association tests. *Nat Genet* **54**, 1466-1469 (2022).
17. Clarke, B. *et al.* Integration of variant annotations using deep set networks boosts rare variant association testing. *Nat Genet* **56**, 2271-2280 (2024).
18. Fiziev, P.P. *et al.* Rare penetrant mutations confer severe risk of common diseases. *Science* **380**, eabo1131 (2023).
19. Sugasawa, S. & Noma, H. Efficient testing and effect size estimation for set-based genetic association inference via semiparametric multilevel mixture modeling. *Biom J* **64**, 1142-1152 (2022).
20. Lali, R. *et al.* Calibrated rare variant genetic risk scores for complex disease prediction using large exome sequence repositories. *Nat Commun* **12**, 5852 (2021).

21. Cheng, J. *et al.* Accurate proteome-wide missense variant effect prediction with AlphaMissense. *Science* **381**, eadg7492 (2023).
22. Gao, H. *et al.* The landscape of tolerated genetic variation in humans and primates. *Science* **380**, eabn8153 (2023).
23. Lippert, C. *et al.* FaST linear mixed models for genome-wide association studies. *Nat Methods* **8**, 833-5 (2011).
24. Gilmour, A.R., Thompson, R. & Cullis, B.R. Average information REML: An efficient algorithm for variance parameter estimation in linear mixed models. *Biometrics* **51**, 1440-1450 (1995).
25. Zhou, W. *et al.* Efficiently controlling for case-control imbalance and sample relatedness in large-scale genetic association studies. *Nat Genet* **50**, 1335-1341 (2018).
26. Chen, H. *et al.* Control for Population Structure and Relatedness for Binary Traits in Genetic Association Studies via Logistic Mixed Models. *Am J Hum Genet* **98**, 653-66 (2016).
27. Robinson, G.K. That BLUP is a Good Thing: The Estimation of Random Effects. *Statistical Science* **6**, 15-32, 18 (1991).
28. Henderson, C.R. Best Linear Unbiased Estimation and Prediction under a Selection Model. *Biometrics* **31**, 423-447 (1975).
29. Maier, R.M. *et al.* Improving genetic prediction by leveraging genetic correlations among human diseases and traits. *Nat Commun* **9**, 989 (2018).
30. Chen, C.Y., Han, J., Hunter, D.J., Kraft, P. & Price, A.L. Explicit Modeling of Ancestry Improves Polygenic Risk Scores and BLUP Prediction. *Genet Epidemiol* **39**, 427-38 (2015).
31. Firth, D. Bias Reduction of Maximum Likelihood Estimates. *Biometrika* **80**, 27-38 (1993).
32. Graham, S.E. *et al.* The power of genetic diversity in genome-wide association studies of lipids. *Nature* **600**, 675-679 (2021).
33. Zheng, Z. *et al.* Leveraging functional genomic annotations and genome coverage to improve polygenic prediction of complex traits within and between ancestries. *Nat Genet* **56**, 767-777 (2024).
34. Ge, T., Chen, C.Y., Ni, Y., Feng, Y.A. & Smoller, J.W. Polygenic prediction via Bayesian regression and continuous shrinkage priors. *Nat Commun* **10**, 1776 (2019).
35. Pathan, N. *et al.* A method to estimate the contribution of rare coding variants to complex trait heritability. *Nat Commun* **15**, 1245 (2024).
36. Casella, G. & Hwang, J.T.G. Shrinkage Confidence Procedures. *Statistical Science* **27**, 51-60 (2012).
37. Keller, J.P. & Rice, K.M. Selecting Shrinkage Parameters for Effect Estimation: The Multi-Ethnic Study of Atherosclerosis. *Am J Epidemiol* **187**, 358-365 (2018).
38. van Zwet, E.W., Tian, L. & Tibshirani, R. Evaluating a shrinkage estimator for the treatment effect in clinical trials. *Stat Med* **43**, 855-868 (2024).
39. Bland, J.M. & Altman, D.G. Multiple significance tests: the Bonferroni method. *BMJ* **310**, 170 (1995).
40. Benjamini, Y. & Hochberg, Y. Controlling the False Discovery Rate - a Practical and Powerful Approach to Multiple Testing. *Journal of the Royal Statistical Society Series B-Statistical Methodology* **57**, 289-300 (1995).
41. Efird, J.T. & Nielsen, S.S. A method to compute multiplicity corrected confidence intervals for odds ratios and other relative effect estimates. *Int J Environ Res Public Health* **5**, 394-8 (2008).

42. Sundaram, L. *et al.* Predicting the clinical impact of human mutation with deep neural networks. *Nat Genet* **50**, 1161-1170 (2018).
43. Frommlet, F. & Nuel, G. An Adaptive Ridge Procedure for L0 Regularization. *PLoS One* **11**, e0148620 (2016).
44. Backman, J.D. *et al.* Exome sequencing and analysis of 454,787 UK Biobank participants. *Nature* **599**, 628-634 (2021).
45. Berry, M.W. Large-Scale Sparse Singular Value Computations. *International Journal of Supercomputer Applications and High Performance Computing* **6**, 13-49 (1992).
46. Pazokitoroudi, A. *et al.* Efficient variance components analysis across millions of genomes. *Nat Commun* **11**, 4020 (2020).
47. Mbatchou, J. *et al.* Computationally efficient whole-genome regression for quantitative and binary traits. *Nat Genet* **53**, 1097-1103 (2021).
48. Wang, X. Firth logistic regression for rare variant association tests. *Front Genet* **5**, 187 (2014).
49. Dey, R., Schmidt, E.M., Abecasis, G.R. & Lee, S. A Fast and Accurate Algorithm to Test for Binary Phenotypes and Its Application to PheWAS. *Am J Hum Genet* **101**, 37-49 (2017).
50. Breslow, N.E. & Clayton, D.G. Approximate Inference in Generalized Linear Mixed Models. *Journal of the American Statistical Association* **88**, 9-25 (1993).
51. Karczewski, K.J. *et al.* The mutational constraint spectrum quantified from variation in 141,456 humans. *Nature* **581**, 434-443 (2020).
52. Wu, P. *et al.* Mapping ICD-10 and ICD-10-CM Codes to Phecodes: Workflow Development and Initial Evaluation. *JMIR Med Inform* **7**, e14325 (2019).

747 **Figures Legends**

748 **Fig. 1. Overview of RareEffect.**

749 **Fig. 2. Estimated signed heritability for lipid phenotypes using 392,748 White British**
750 **samples in UK Biobank whole exome sequencing data**

751 **Fig. 3. Variant-level effect size on HDL cholesterol for variants in *APOC3* gene (chromosome**
752 **11) and *SLC12A3* gene (chromosome 16)**

753 **Fig. 4. Comparison of performance of risk prediction models for lipid phenotypes using**
754 **314,198 White British samples (80% of the whole White British samples) in UK Biobank**
755 **whole exome sequencing data**

Fig. 1. Overview of RareEffect.

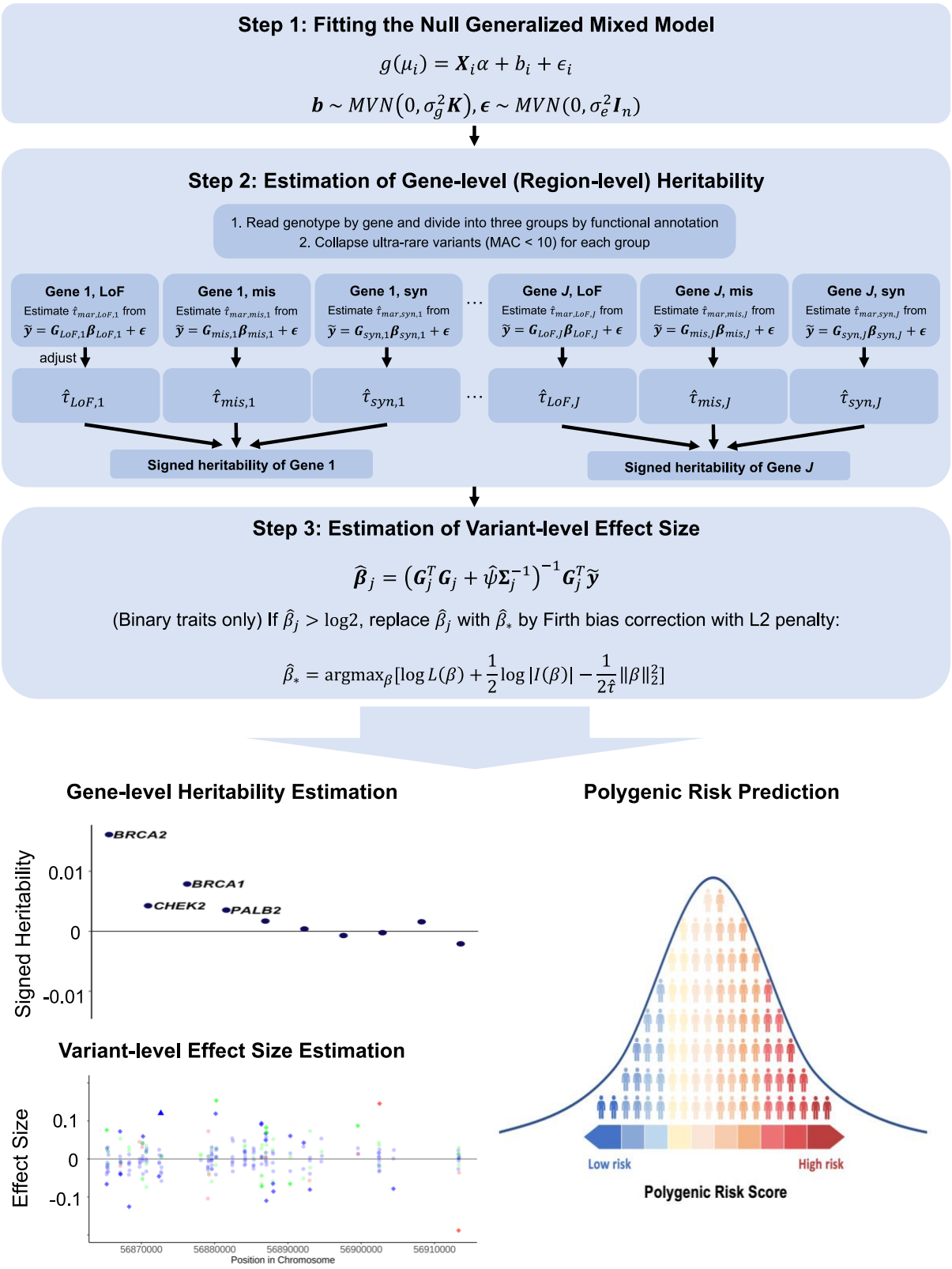

RareEffect encompasses three steps. In step 1, we fit a null GLMM using AI-REML approach, and obtain residuals for the subsequent steps. In step 2, we divide variants by gene and its functional annotation (LoF, missense, and synonymous). We first estimate the variance

component of each group and adjust them using MoM approach. In step 3, we calculate the variant-level effect size using BLUP estimates. For binary traits, Firth bias correction is additionally applied to adjust the case-control imbalance. Through RareEffect, we provide region-level and variant-level effect sizes for enhanced interpretability and improved risk prediction performance.

767 **Fig. 2. Estimated signed heritability for lipid phenotypes using 392,748 White British**
768 **samples in UK Biobank whole exome sequencing data**
769

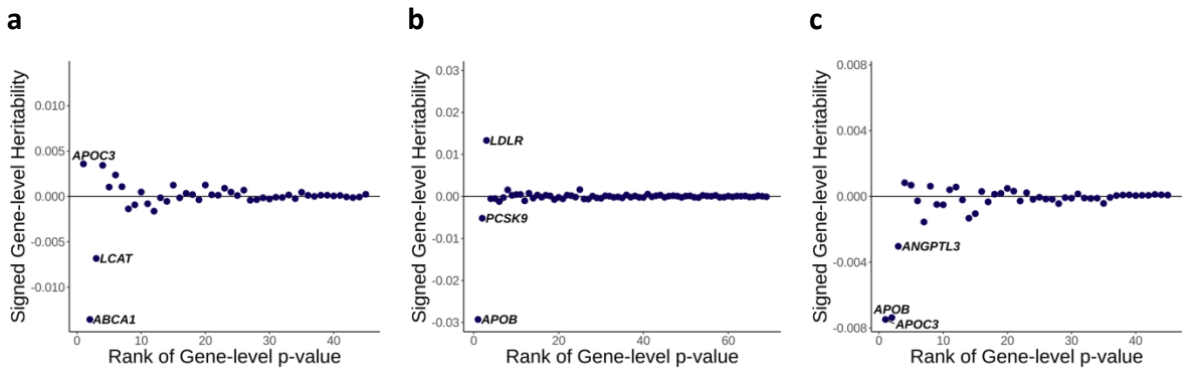

770 Signed gene-level heritability from RareEffect for (a) HDL cholesterol level, (b) LDL
771 cholesterol level, and (c) triglycerides level. Gene-level p-values were obtained from SAIGE-
772 GENE+, and we included genes with p-values < 2.5×10^{-6}. The x-axis represents the rank
773 order of genes based on their gene-level p-values. Lower ranks correspond to genes with
774 more significant p-values. The y-axis shows the signed gene-level heritability for each gene.
775 Signed heritability indicates the direction (positive or negative) and magnitude of the genetic
776 contribution of the gene to the trait.

Fig. 3. Variant-level effect size on HDL cholesterol for variants in *APOC3* gene (chromosome 11) and *SLC12A3* gene (chromosome 16).

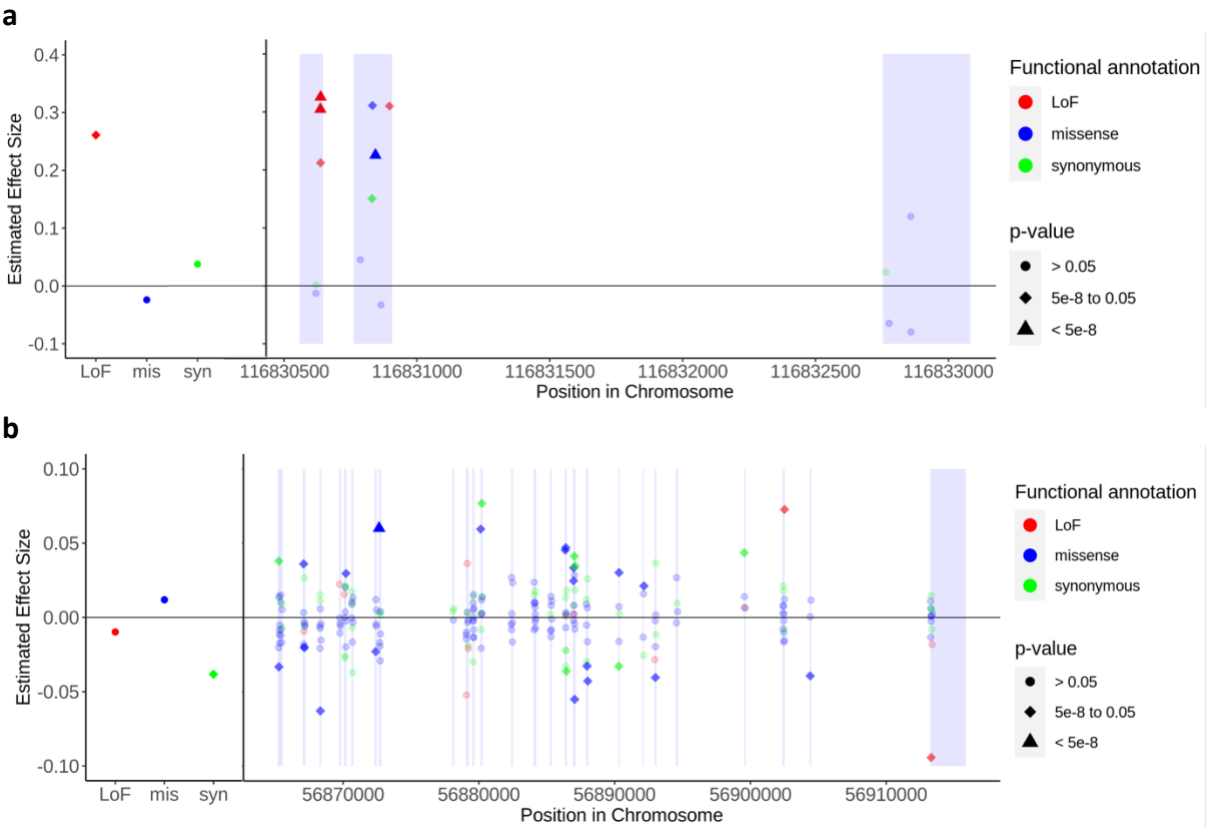

Variant-level effect size on HDL cholesterol level for (a) *APOC3* and (b) *SLC12A3* genes. Gene-level p-values were obtained from SAIGE-GENE+, and we included genes with p-values < 2.5×10^{-6}. The left panel shows the effect size of collapsed ultra-rare variants categorized by their functional annotations: loss-of-function (LoF), missense, and synonymous, respectively. The right panel displays the variant-level effect size of rare variants. Variants are color-coded based on their functional annotation: red for LoF, blue for missense, and green for synonymous. The shapes of the points indicate the significance of the variants: circles represent p-values > 0.05, diamonds represent p-values between 5×10^{-8} and 0.05, and triangles represent p-values < 5×10^{-8}. Single-variant p-values were obtained from SAIGE, while the p-values of collapsed variants were derived from linear regression by regressing $\tilde{y}$ on each collapsed variant. The exon region is shaded.

Fig. 4. Comparison of performance of risk prediction models for lipid phenotypes using 314,198 White British samples (80% of the whole White British samples) in UK Biobank whole exome sequencing data.

a

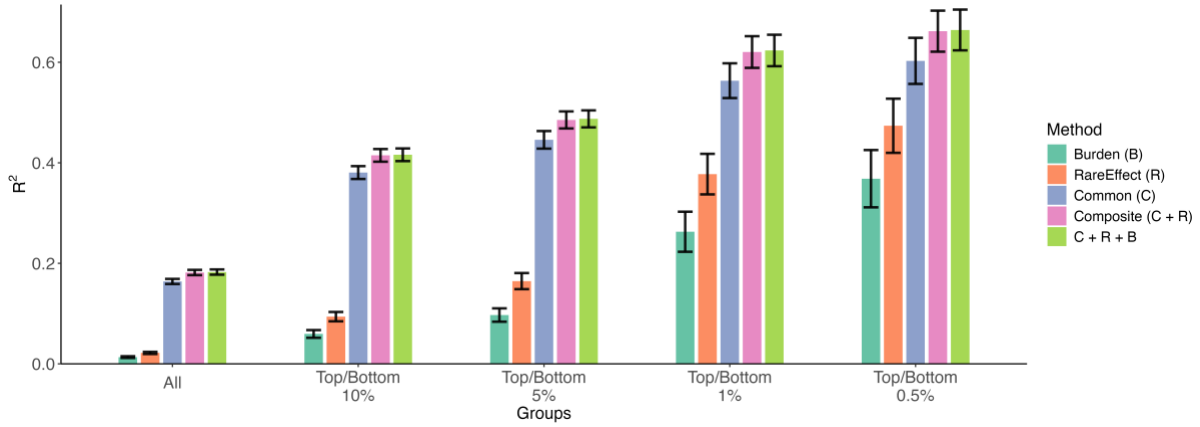

b

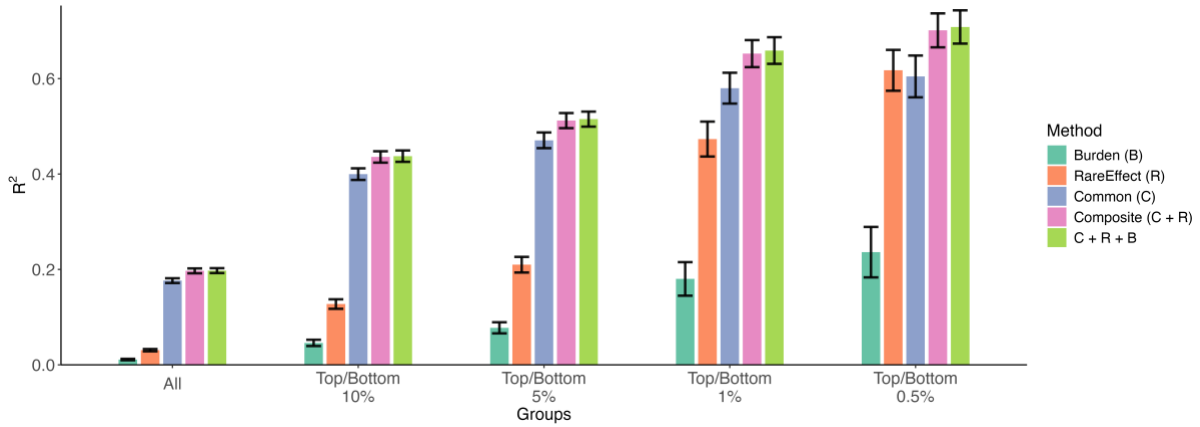

c

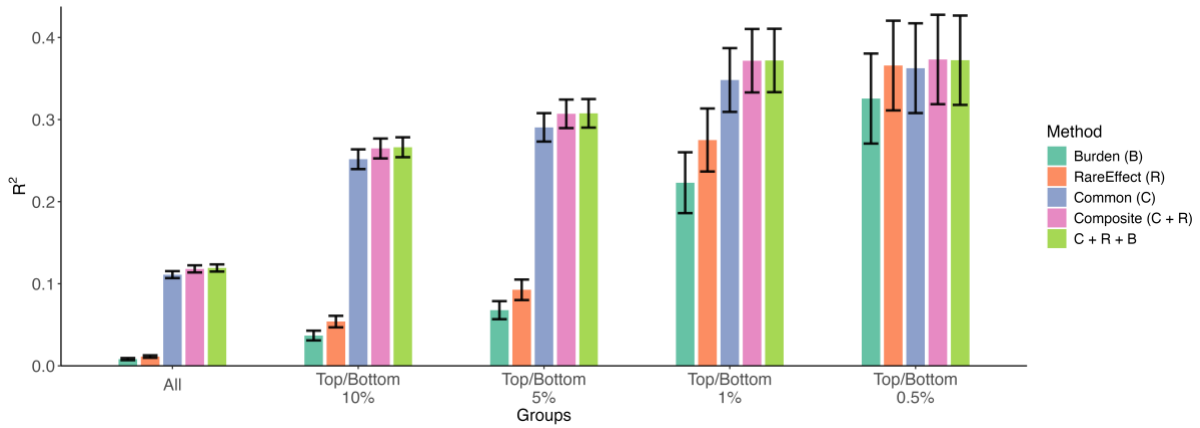

Predictive performance was evaluated using the coefficient of determination (R^2) of the risk prediction models for (a) HDL cholesterol level, (b) LDL cholesterol level, and (c) Triglycerides

level. We evaluated the performance of five models using: (1) PRS_{burden} only, (2) PRS_{RE} only, (3) PRS_{common} only, (4) composite score, (5) $PRS_{common} + PRS_{RE} + PRS_{burden}$ by five subgroups: (1) all samples, (2) samples with top/bottom 10% PRS, (3) samples with top/bottom 5% PRS, (4) samples with top/bottom 1% PRS, and (5) samples with top/bottom 0.5% PRS. The black vertical lines represent the 95% confidence interval of the R^2 estimates.

Supplementary Figures

1. Estimated signed heritability for 10 tested traits
2. Predictive performance for 10 tested traits
3. Relationship between common variant PRS (PRS_{common}) and RareEffect PRS (PRS_{RE})
4. Comparison of the performance of rare variant PRS methods for lipid phenotypes
5. Comparison of the performance of rare variant PRS methods when combined with common variant PRS (SBayesRC) for lipid phenotypes
6. Enrichment of high-risk individuals based on RareEffect PRS (PRS_{RE}), common variant PRS (PRS_{common}) and the composite score among phenotype outliers
7. Computation time of RareEffect, linear regression, and ridge regression
8. Memory usage of RareEffect by number of variants
9. Computation time of the fast implementation Firth bias correction and the standard Firth correction
10. Relationship between RareEffect PRS (PRS_{RE}) and phenotype values
11. Comparison of estimated variance components between RareEffect and the MoM estimator
12. Comparison of estimated effect sizes between computing the hat matrix at every iteration and computing it only once in Firth bias correction
13. Distribution of RareEffect PRS

Supplementary Tables

1. List of 100 analyzed traits in the UK Biobank
2. Predictive performance measured by R^2 and AUC for the analyzed phenotypes in the UK Biobank
3. Predictive performance measured by mean/prevalence difference and enrichment for the analyzed phenotypes in the UK Biobank
4. Number of phenotypes showing improvement compared to common PRS performance
5. Comparison of predictive performance between RareEffect and DeepRVAT, AlphaMissense, and PrimateAI-3D
6. Pearson correlation between PRS from common variants and RareEffect PRS
7. Estimation performance for simulated continuous data across scenarios

8. p-values from paired t-tests for the difference in MSE
9. Estimation performance for simulated binary data across scenarios
10. Predictive performance for simulated data across scenarios
11. Estimation performance for gene-level heritability
12. Estimated gene-level heritability by sample size
13. Proportion of conservative estimates in confidence interval coverage failures
14. Estimated signed heritability by genetic sex for the top 10 genes
15. Proportion of negative MoM estimates of variance components
16. p-values from DeLong's test for differences in AUROC
17. Predictive performance for continuous phenotypes in the UK Biobank after excluding the top 3 genes
18. Comparison of predictive performance stratified by genetic sex
19. Direction of estimated gene-level heritability
20. Comparison of predictive performance with adaptive ridge adjustment